Metrol. Meas. Syst., Vol. 27 (2020) No. 2, pp. 323–337
DOI: 10.24425/mms.2020.132778

METROLOGY AND MEASUREMENT SYSTEMS
Index 330930, ISSN 0860-8229
www.metrology.wat.edu.pl

COMPARATIVE STUDIES OF THE OPTICAL ABSORPTION COEFFICIENT SPECTRA IN THE IMPLANTED LAYERS IN SILICON WITH THE USE OF NONDESTRUCTIVE SPECTROSCOPIC TECHNIQUES

Krzysztof Dorywalski[1)], Łukasz Chrobak[2)], Mirosław Maliński[2)]

1) *Koszalin University of Technology, Faculty of Mechanical Engineering, Department of Mechatronics and Automation, Śniadeckich 2, 75-453 Koszalin, Poland* (✉ *krzysztof.dorywalski@tu.koszalin.pl*, +48 94 348 6533)
2) *Koszalin University of Technology, Faculty of Electronics and Computer Sciences, Śniadeckich 2, 75-453 Koszalin, Poland*

Abstract

This work presents results of comparative studies of the optical absorption coefficient spectra of ion implanted layers in silicon. Three nondestructive and noncontact techniques were used for this purpose: spectroscopic ellipsometry (SE), modulated free carriers absorption (MFCA) and the photo thermal radiometry (PTR). Results obtained with the ellipsometric method are the proof of correctness of the results obtained with the MFCA and PTR techniques. These techniques are usually used for investigations of recombination parameters of semiconductors. They are not used for investigations of the optical parameters of semiconductors. Optical absorption coefficient spectra of Fe^+ and Ge^+ high energy and dose implanted layers in silicon, obtained with the three techniques, are presented and compared.

Keywords: silicon, ion implantation, optical absorption coefficient spectra, modulated free carrier absorption, photo thermal radiometry, ellipsometry, nondestructive techniques.

1. Introduction

Nowadays the ion implantation is still an important tool in modern electronics [1–4]. Influence of the implantation process on different physical parameters is measured with several techniques. In this paper Fe^+ and Ge^+ ion-implanted silicon samples are investigated. Reaction of iron and silicon during ion implantation is reported in [5]. Issues of recrystallization behavior and thermal annealing of silicon samples implanted with iron are described in [6, 7]. Results of the low-energy Fe^+ ion implantation into silicon nanostructures are reported in [8]. In turn, ferromagnetic behavior of Fe^+ implanted Si is presented in [9]. Results of investigations of silicon implanted with Ge^+ ions after annealing are reported in [10–12]. Ion implantation damage and crystalline-amorphous transition in Ge are discussed in [13]. Thermal oxidation of Ge-implanted Si and the role of defects are reported in [14].

In this paper three measuring techniques are considered and compared: *spectroscopic ellipsometry* (SE), *modulated free carriers absorption* (MFCA) and the *photo thermal radiometry* (PTR). Modulated free carriers absorption is a technique routinely applied to characterize materials recombination parameters such as the lifetime of carriers [15–18]. It is not routinely applied to measurements of optical properties such as coefficient spectra of optical absorption. Photo thermal radiometry is a technique applied to characterize materials recombination and thermal parameters [19–23]. A comparison of these methods from the point of view of investigations of recombination parameters in silicon is presented in paper [24]. Both the MFCA and PTR techniques proved appropriate tools for investigating properties of implanted layers [25–29]. Spectroscopic ellipsometry is a well-established optical technique, routinely applied to characterize materials optical and structure properties [30]. As non-destructive, non-invasive and highly sensitive to changes of optical properties, ellipsometry is one of the most suitable methods for studies of implanted materials. The technique has already been applied for the investigations of the optical constants' modification and the process of amorphization of silicon due to the ion implantation [31–35], as well as for the characterization of a damage profile [36, 37].

2. Sample preparation and experimental methods

In our research, we used silicon p-type samples. The samples had been grown using the Czochralski method. The samples exhibited the (1 1 1) orientation. The concentration of the Boron dopant and resistivity of the samples were 10^{15} cm^{-3} and 10 Ω·cm respectively. After standard cleaning and polishing, wafers were cut into square 5 mm × 5 mm × 0.375 mm samples. Fe+, Ge+ ions were introduced into silicon samples. The energy of implantation was 100 keV. The doses of ions were about 10^{14} cm^{-2}. The implanted area had the same size in the all samples *i.e.* 2 mm × 2 mm.

The experimental setup for modulated free carriers absorption method measurements is presented schematically in Fig. 1 and described in details elsewhere [26]. This setup allows for spatial profile measurements of the MFCA signal in the frequency domain.

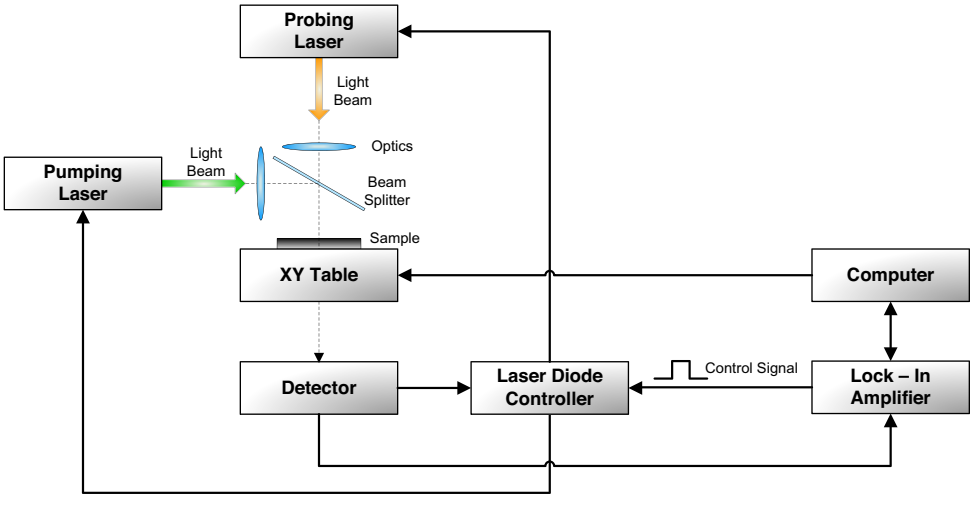

Fig. 1. Block diagram of the experimental set-up used for investigations of the MFCA frequency characteristics and the spatial profile distribution measurements.

Metrol. Meas. Syst., Vol. 27 (2020), No. 2, pp. 323–337
DOI: 10.24425/mms.2020.132778

The experimental setup for photo thermal radiometry method measurements is presented schematically in Fig. 2 and described in details elsewhere [29]. This setup allows for spatial profile measurements of the PTR signal and its measurements in the frequency domain.

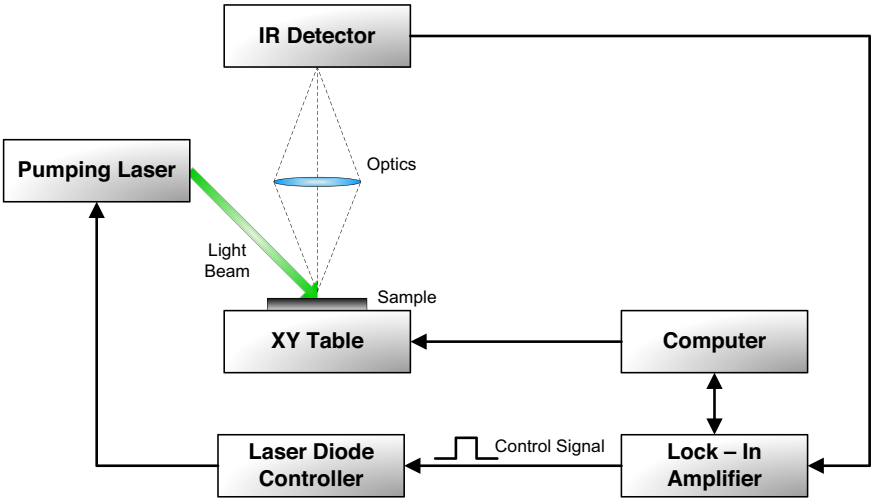

Fig. 2. Block diagram of the experimental set-up used for the PTR frequency characteristics and spatial profile distribution measurements.

The ellipsometric spectra $\Psi(E)$ and $\Delta(E)$ of the implanted Si samples were recorded at room temperature in the photon energy range 0.75–6.4 eV with the resolution of about 0.03 eV using a Woollam RC2 dual rotating compensator ellipsometer. For high accuracy of the subsequent experimental data analysis, the measurements were applied at multiple angles of the incident light. The spectra of the Mueller matrix elements reveal that no mode conversion by either the optical anisotropy nor the light depolarization is present. Thus, the discussion below will be restricted to Ψ and Δ. Additionally, the surface roughness of the studied specimens was measured with atomic force microscopy AFM (with a Park XE-150 device).

3. Theoretical background

MFCA and PTR signals strongly depend on the lifetime of carriers. With the decreasing lifetime of carriers, there is a strong decrease of the amplitude of the signal. The lifetime of carriers as well as their diffusion length in the implanted layer are much smaller than in the silicon substrate. In sum, the measured signal comes mainly from the silicon substrate (see Fig. 3). The ion implantation causes also a significant increase of the optical absorption coefficient in the implanted layer as compared to the substrate.

A simplified model which describes the dependence $k(E)$ results from the Lambert–Beer law which says that the intensity of light passing through a sample of the thickness l is described as:

$$I(E) = I_0 \exp\left[-\beta(E) \cdot l\right], \tag{1}$$

so for the MFCA measurements

$$k(E) = \frac{\mathrm{MFCA}_i(E)}{\mathrm{MFCA}_s(E)} = \exp\left[-n_\beta \cdot \beta_s(E) \cdot d\right] \tag{2}$$

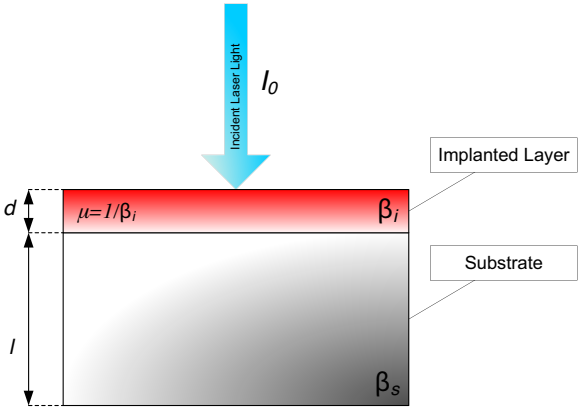

Fig. 3. Simplified diagram of the implanted sample under the laser beam excitation. Symbols are as follows: I_0 – the intensity of the excitation light, β_i – the optical absorption coefficient in the implanted layer, β_s – the optical absorption coefficient in the silicon substrate, d – the thickness of the implanted layer, l – the total thickness of the sample, μ – the optical absorption path.

or for the PTR measurements

$$k(E) = \frac{\mathrm{PTR}_i(E)}{\mathrm{PTR}_s(E)} = \exp\left[-n_\beta \cdot \beta_s(E) \cdot d\right], \tag{3}$$

$$\beta_i(E) = n_\beta \cdot \beta_s(E) = n_\beta \cdot A \cdot \left(E - E_g\right)^2, \tag{4}$$

where: E – photon energy, n_β – increase coefficient of the optical absorption coefficient in the implanted layer compared to the silicon substrate, A – absorption factor for silicon. Indices in the equations are the following: i – implanted layer, s – substrate, d – thickness of the implanted layer.

The proposed simplified model can be used for interpretation of results obtained with the MFCA and PTR methods for silicon samples implanted with various ions under two conditions. The first condition is that the diffusion length of carriers in the implanted layer is much smaller than its thickness. This information is obtained from the frequency measurements of the MFCA or PTR characteristics. The second condition is that the amplitudes of the MFCA and PTR signals must be read out at a frequency where the plasma components dominate in the frequency characteristics.

In ellipsometry, information about material and geometrical properties can be deduced from the measurement of the change of the light polarization state after interaction with the sample under study [38–42]. A diagram of the ellipsometric measurement is shown in Fig. 4.

The sample is illuminated at the oblique incidence angle with light of known polarization. The measured reflected light polarization state is described by two parameters, Ψ and Δ, which refer to the arc tan of the amplitude ratio and the phase shift respectively, of p- and s-components of polarized light as described by the fundamental equation of ellipsometry [30, 43].

$$\rho = \tan\Psi e^{i\Delta} = \frac{R_p}{R_s} = \frac{E_{rp}/E_{ip}}{E_{rs}/E_{is}}, \tag{5}$$

where R_p and R_s are the Fresnel reflection coefficients.

Metrol. Meas. Syst., Vol. 27 (2020), No. 2, pp. 323–337
DOI: 10.24425/mms.2020.132778

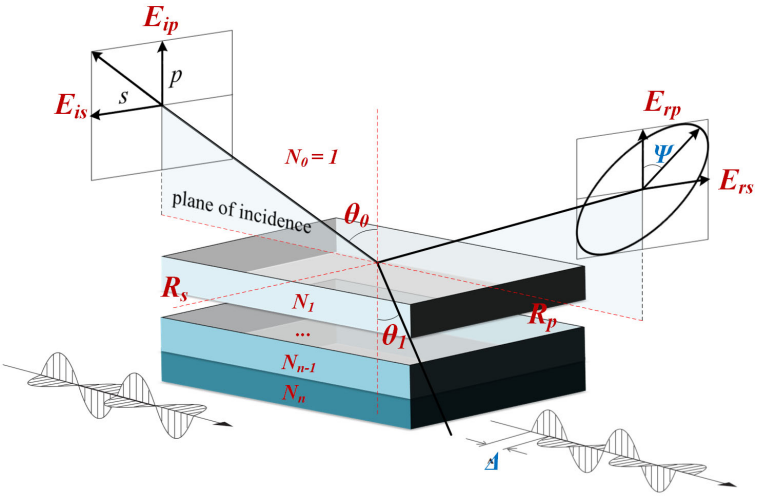

Fig. 4. Diagram of an ellipsometric measurement. The sample is illuminated at the oblique incidence angle θ_0 (θ_1 is the angle of refraction) with the polarized light. The polarization state of the measured reflected light depends on the optical properties (complex refractive index N) of the sample and thicknesses of the layers in the case of the layered sample. Symbols E_{ip}, E_{is} denote p- and s-components of the incidence polarized light, where E_{rp} and E_{rs} are components of the reflected light, and R_p and R_s reflection coefficients of p- and s-polarization, respectively.

Once the $\Psi(E)$ and $\Delta(E)$ spectra are measured the samples parameters of interest are determined by the transfer matrix calculus in the process of a nonlinear least-squares numerical inversion of experimental data, assuming the parameterized optical model which consists of plan-parallel layers, each described by its optical constants and thickness. Ellipsometry on implanted materials is based on the fact that the implantation substantially changes their optical properties [44]. In the most common case of the implantation of the crystalline material at a relatively high energy (more than 10 keV), amorphization of the implanted area occurs and, obviously, the amorphous medium has very different optical properties from the crystalline one. However, as was recently shown, even in the case of low energy ion implantation (around 1 are keV), where no amorphization is observed, implantation-induced damages change optical constants of the media which, thanks to their high precision, can be observed with ellipsometry [45–47].

4. Results and discussion

The thickness of the implanted layer necessary for calculations of the optical absorption coefficient of the implanted layer from the MFCA and PTR measurements was calculated using the TRIM software. The Fe^+ and Ge^+ ions distributions are presented in Fig. 5 and Fig. 6, respectively.

The thickness of the implanted layer was 174 nm for a sample implanted with iron ions and 149 nm for a sample implanted with germanium ions.

Optical absorption coefficient spectra of crystalline silicon, amorphous silicon, Si:Fe^+ implanted layer determined by the MFCA method are presented in Fig. 7.

Optical absorption coefficient spectra of: crystalline silicon, amorphous silicon, Si:Ge^+ implanted layer, determined by the MFCA method are presented in Fig. 8.

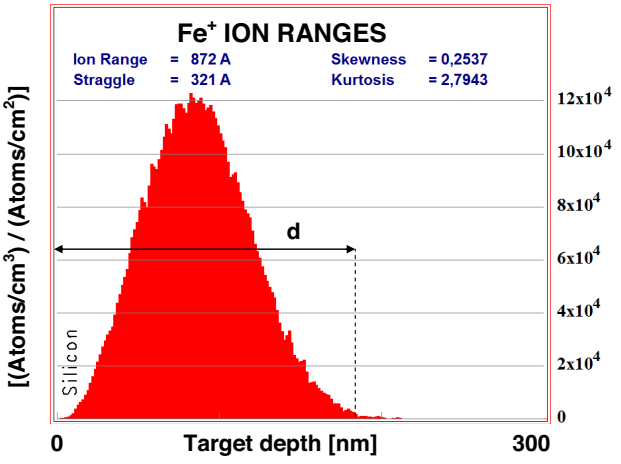

Fig. 5. Distribution of Fe^+ ions in silicon computed in the TRIM software. The thickness of the implanted region d is about 174 nm.

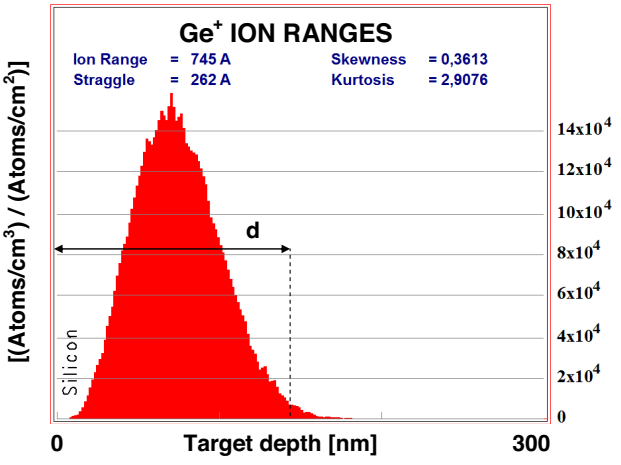

Fig. 6. Distribution of Ge^+ ions in silicon computed in the TRIM software. The thickness of the implanted region d is about 149 nm.

Optical absorption coefficient spectra of: crystalline silicon, amorphous silicon, Si:Fe^+ implanted layer, determined by the PTR method are presented in Fig. 9.

Optical absorption coefficient spectra of: crystalline silicon, amorphous silicon, Si:Ge^+ implanted layer, determined by the PTR method are presented in Fig. 10.

From the results obtained with the use of the MFCA and PTR methods, it is easy to conclude that the increase of the optical absorption coefficient in the implanted layer is bigger than in the case of literature references concerning the amorphous silicon. The obtained results needed experimental verification so the ellipsometric measurements are performed. They were treated as the reference measurement results.

Metrol. Meas. Syst., Vol. 27 (2020), No. 2, pp. 323–337
DOI: 10.24425/mms.2020.132778

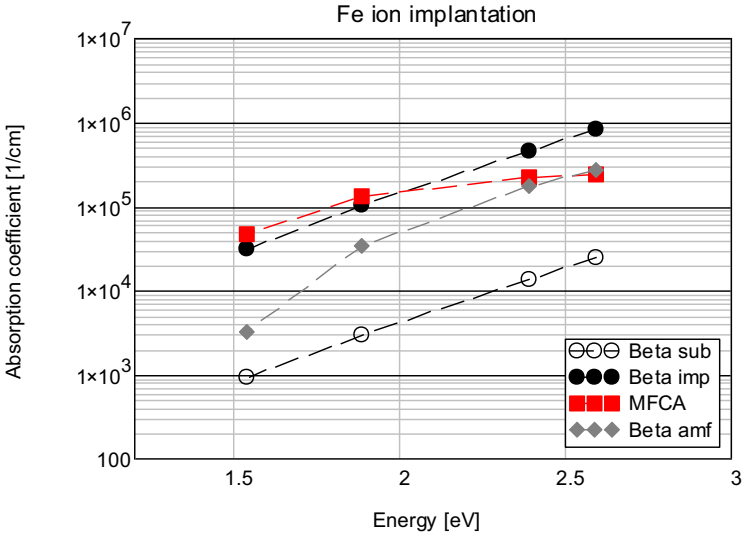

Fig. 7. Optical absorption coefficient values for silicon samples implanted with Fe^+ ions obtained from MFCA spectral measurements (full squares). Circles – theoretical optical absorption coefficient spectra of implanted silicon (full circles) and non-implanted silicon (empty circles). Diamonds – optical absorption coefficient spectrum of an amorphous silicon [51].

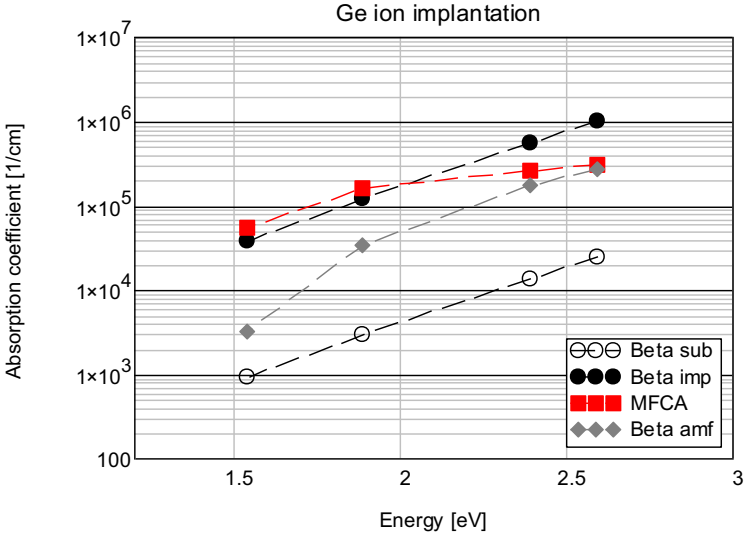

Fig. 8. Optical absorption coefficient values for silicon samples implanted with Ge^+ ions obtained from MFCA spectral measurements (full squares). Circles – theoretical optical absorption coefficient spectra of implanted silicon (full circles) and non-implanted silicon (empty circles). Diamonds – optical absorption spectrum coefficient of an amorphous silicon [51].

In the case of crystalline silicon (c–Si), the presence of SiO_2 on the top of Si after exposure to air needs to be taken into consideration as an additional layer, beside the implanted region of the sample (i–Si), in the optical model. Having in mind that optical constants of these three

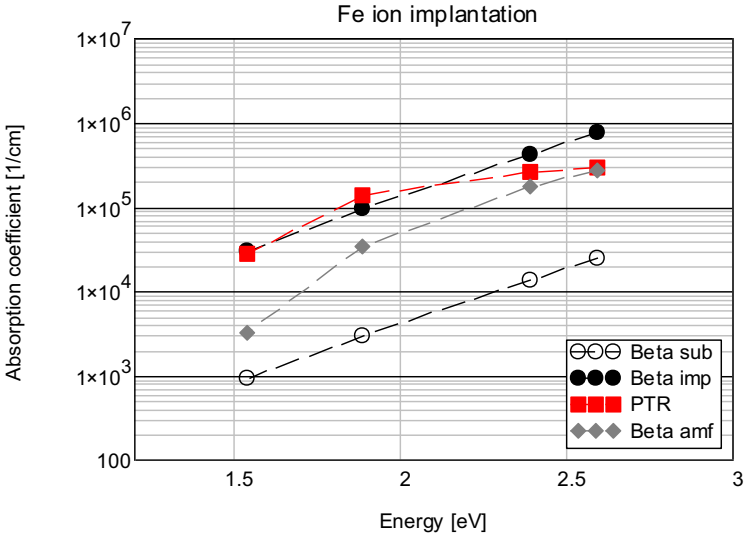

Fig. 9. Optical absorption coefficient values for silicon samples implanted with Fe^+ ions obtained from PTR spectral measurements (full squares). Circles – theoretical optical absorption coefficient spectra of implanted (full circles) and non-implanted silicon (empty circles). Diamonds – optical absorption coefficient spectrum of amorphous silicon [51].

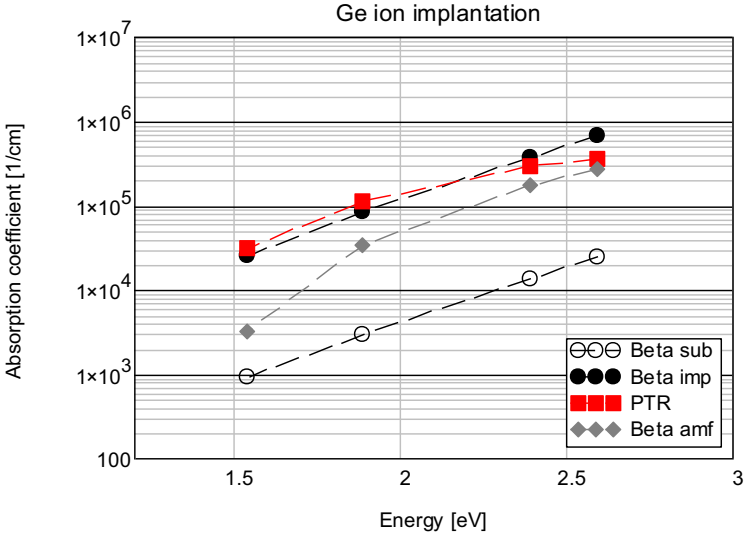

Fig. 10. Optical absorption coefficient values for silicon samples implanted with Ge^+ ion obtained from PTR spectral measurements (squares). Circles – theoretical optical absorption coefficient spectra of implanted silicon (full circles) and non-implanted silicon (empty circles), Diamonds – optical absorption coefficient spectrum of amorphous silicon [51].

materials are significantly different [44], thicknesses of the top layer of the implanted region $i-$Si and SiO_2 can be determined using the so-called 5-phase model: $c-$Si/$i-$Si/SiO_2/BEMA where BEMA stands for the additional layer which describes surface roughness of the sample according

Metrol. Meas. Syst., Vol. 27 (2020), No. 2, pp. 323–337
DOI: 10.24425/mms.2020.132778

to the Brugemann Medium Approximation [30] theory. The non-implanted region of the samples was also measured and its optical constants determined to ensure that the reference data for Si and SiO_2 can be applied to data modeling. Since the effect of implantation on the optical properties of SiO_2 is minor [48], it was assumed that its optical constants were not modified due to implantation.

Finally, in order to ensure a unique fit between experimental and simulated data, the optical constants of the i–Si layer were described by a parametric dispersion function model. Among various dispersion functions, Tauc–Lorentz (T–L) [49] and Cody–Lorentz (C–L) [50] are the most commonly applied to the amorphous materials. Both describe the main absorption of the material using a broad Lorentzian line shape with zero absorption below the bandgap. However, as the C–L oscillator also includes the Urbach absorption term to model absorption below the bandgap, this model was chosen. To find good starting points, the parameters of C–L model were first fitted to the reference data for the amorphous silicon [51]. Afterwards, all C–L model parameters together with thicknesses of the implanted SiO_2 and roughness layers, $d_{i\text{–Si}}$, d_{SiO_2}, d_r, respectively, were varied to match the experimental and simulated data. The standard Levenberg–Marquardt routine, as implemented in the CompleteEASE^{TM} software, was used to fit model parameters [52].

Results of the fitting procedure of ellipsometric data for Fe^+ and Ge^+ implanted silicon samples are shown in Fig. 11 and Fig. 12 where solid and dotted lines denote modeled and experimental

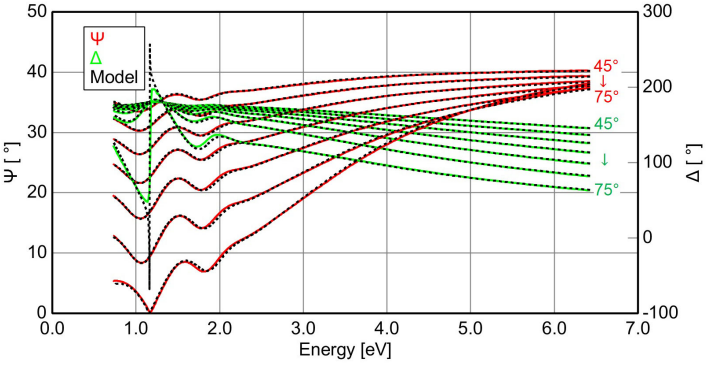

Fig. 11. Model (dots) and experimental (solid lines) Ψ, Δ ellipsometric spectra of an Fe^+ implanted silicon sample for angles of the incident light from 45° to 75° with a step 5°.

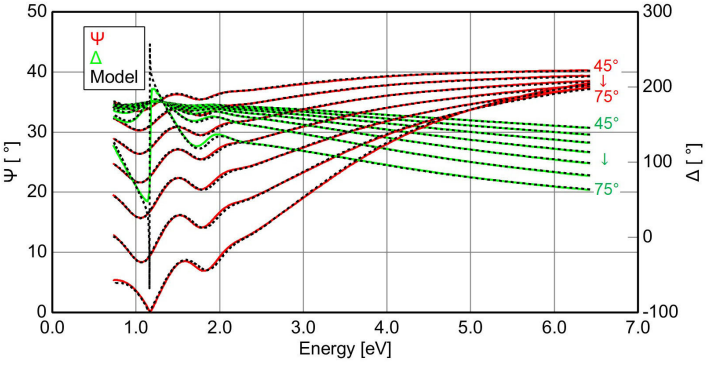

Fig. 12. Model (dots) and experimental (solid lines) Ψ, Δ ellipsometric spectra of a Ge^+ implanted silicon sample for angles of the incident light from 45° to 75° with a step 5°.

data, respectively. Interference fringes in the ellipsometric spectra below the photon energy range ~2.5 eV indicate the light reflection at the $i-$Si/Si interface. Therefore, the thicknesses of all modeled layers can be determined based on the ellipsometric data analysis in this energy range.

It should be noted that optical constants of the implanted region are in principle vertically inhomogeneous [36]. The variation of the complex refractive index with the depth of the film can be modeled as a layer structure where each layer is described by the composition of amorphous and crystalline Si according to the effective medium theory [37]. Such sophisticated modeling gives a chance to obtain the ion implantation-induced damage depth profile [36]. Nevertheless, a very good match between experimental and theoretical curves, as shown in Figs. 11 and 12, with the average mean square error *MSE* around 4 proves that a much simpler theoretical model in which the implanted region is expressed as a layer with parameterized optical function (C–L oscillator) can be successfully applied in ellipsometric studies of ion implanted Si.

The determined real n and imaginary k parts of the complex refractive index of the Fe^+ and Ge^+ implanted silicon regions for all the samples studied are shown in Fig. 13.

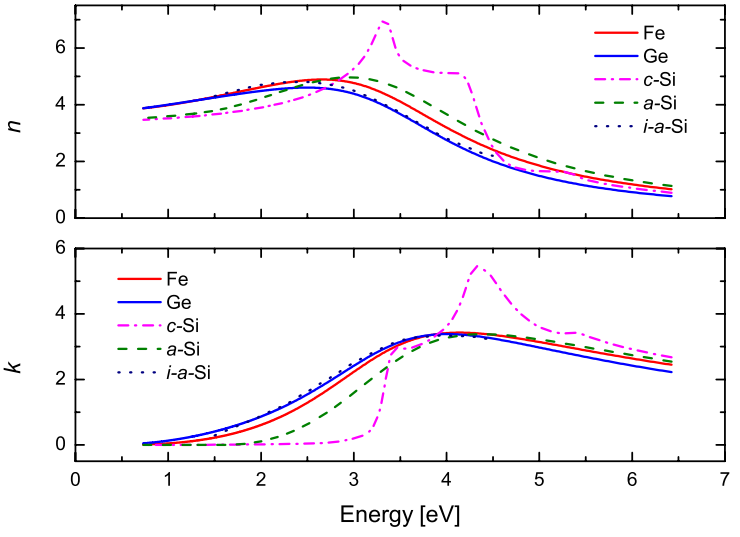

Fig. 13. Real n and imaginary k parts of the complex refractive index of Fe^+ and Ge^+ implanted silicon samples determined after numerical inversion of ellipsometric data. Data for crystalline $c-$Si [51], amorphous $a-$Si [51] and self-implanted $i-a-$Si [33] silicon are plotted for comparison.

It can be seen that the optical spectra of the implanted layer are indeed similar to the corresponding spectra for amorphous Si. All the obtained layers thicknesses are collected in Table 1. The determined thicknesses of the roughness layer d_r for all the studied samples are in good agreement with the corresponding root mean square R_q value obtained with AFM.

Table 1. Determined, by the spectroscopic ellipsometry, thicknesses of the implanted $d_{i-\mathrm{Si}}$, SiO_2 $d_{\mathrm{SiO_2}}$, and roughness d_r layers for Fe^+, Ge^+ ion implanted Si samples.

Ion	$d_{i-\mathrm{Si}}$ **[nm]**	$d_{\mathrm{SiO_2}}$ **[nm]**	d_r **[nm]**	R_q **(AFM) [nm]**	***MSE***
Fe+	146.65 ± 0.05	2.77 ± 0.02	6.45 ± 0.09	4.4	5.28
Ge+	113.87 ± 0.05	0.71 ± 0.03	2.58 ± 0.09	2.4	5.43

Metrol. Meas. Syst., Vol. 27 (2020), No. 2, pp. 323–337
DOI: 10.24425/mms.2020.132778

Optical absorption coefficient spectra of: crystalline silicon, amorphous silicon, Si:Ge$^+$ implanted layer, Si:Fe$^+$ implanted layer determined by the ellipsometry method are presented in Fig. 14.

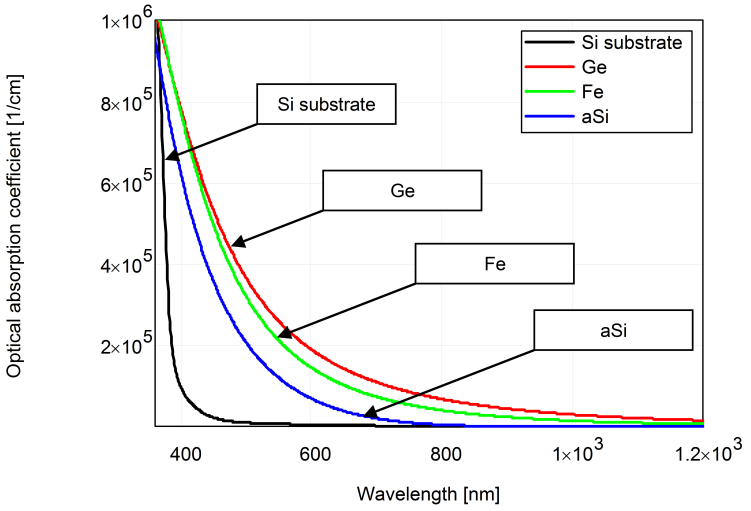

Fig. 14. Optical absorption coefficient spectra of: crystalline silicon, amorphous silicon, Si:Ge$^+$, Si:Fe$^+$ implanted silicon layers calculated from n and k spectra obtained from ellipsometric measurements.

A comparison of values of the n_β parameter, describing the increase of the optical absorption coefficient of the implanted layers respective to the silicon crystalline substrate and defined by equation (4), obtained for Fe$^+$ and Ge$^+$ ions, with different measuring methods is presented in Table 2.

Table 2. Comparison of the values of changes of the optical absorption coefficient in implanted layers, expressed by n_β parameter, determined by MFCA, PTR and ELIP methods.

Ion	d_{TRIM} [nm]	n_β–MFCA fitting	n_β–PTR fitting	n_β–ELIP fitting
Fe$^+$	174	33.94 ± 4.88	35.09 ± 13.11	36.58 ± 5.69
Ge$^+$	149	40.50 ± 4.15	35.30 ± 4.35	40.18 ± 5.15

5. Conclusions

This paper shows a comparison of the results of measurements of the optical absorption coefficient spectra of implanted layers in silicon. For comparison the layers of silicon implanted with a high energy and high dose Fe$^+$ and Ge$^+$ ions were chosen. Three measuring methods *i.e.* the modulated free carrier absorption (MFCA), photo thermal radiometry (PTR) and ellipsometry were chosen for comparison. The ellipsometric method was used as the reference method for to the MFCA and PTR methods.

The following conclusions can be drawn from the experiments. All the three methods gave similar values of the n_β factor, describing the increase of the optical absorption coefficient spectra in the ion implanted layers respective to the crystalline silicon spectra, both for Fe$^+$ and Ge$^+$

ions. It turned out that this factor n_β for the investigated implanted layers is approximately two times bigger than the literature n_β factor for the amorphous silicon ($n_\beta = 17$). This n_β factor for MFCA and PTR methods was extracted in this paper from the experimental $k(E)$ spectra with the simplified model. However, its application is limited to the implanted layers exhibiting a very short diffusion length of carriers. The ellipsometric method does not have this limitation and as such is more universal.

As for practical consequences, a compatibility between modeled and experimental ellipsometric curves shows that the relatively simple optical model proposed here, in which optical response of the implanted region is described by the Cody–Lorentz dispersion formula, can be successfully applied in ellipsometric studies of ion implanted silicon. When compared to the more sophisticated model, in which the implanted region is described with multiple layers with a different ratio of amorphous and crystalline Si, this model substantially reduces the model parameter correlation. Therefore, we believe that the model proposed here can be successfully applied in ellipsometric studies of implanted silicon with any ions.

For MFCA and PTR methods the thickness of the implanted layers must be computed with the TRIM program while in the ellipsometric method it is measured directly. A comparison of the results obtained in this way shows that the thicknesses are similar. The methods used have no limitations in terms of the sample size. The ellipsometric method does not require a calibration curve for the apparatuswhich, unfortunately, is required for MFCA and PTR methods. Considering the cost, the MFCA and PTR methods are much more favorable when compared to the ellipsometric method. As for disadvantages of PTR, it requires precise optics focusing infrared radiation on the surface of the detector. In the MFCA technique, the disadvantage is the need to provide a precisely correlated position of two laser beams. To sum up all three methods have their advantages and disadvantages but the comparison presented in this paper shows that the results obtained with these methods are similar at least for the high energy and high dose ion implanted layers.

Acknowledgements

We thank Dr. Nadezhda Kukharchyk for preparation of the silicon implanted samples and Evgeny Krüger from Universität Leipzig for performing ellipsometry measurements. K. Dorywalski gratefully acknowledges the partial funding by the National Science Centre, Poland, under grant no. 2018/02/X/ST5/02508.

References

[1] Tadjer, M.J., Fares, Ch., Mahadik, N.A., Freitas Jr., J.A., Smith D., Sharma R., Law M.E., Ren, F., Pearton, S.J., Kuramata A. (2019). Damage Recovery and Dopant Diffusion in Si and Sn Ion Implanted β–Ga_2O_3. *ECS Journal of Solid State Science and Technology*, 8(7), Q3133–Q3139.

[2] Chalifoux, B.D., Yao, Y., Woller, K.B., Heilmann, R.K.,. Schattenburg, M.L. (2019). Compensating film stress in thin silicon substrates using ion implantation. *Optics Express*, 27(8), 11182–11195.

[3] Hirose, R., Kadono, T., Okuyama, R., Shigematsu, S., Onaka-Masada, A., Okuda, H., Koga, Y., Kurita, K. (2018). Proximity gettering of silicon wafers using CH3O multielement molecular ion implantation technique. *Japanese Journal of Applied Physics*, 57(9), 096503.

[4] Stepanov, A.L., Vorobev, V.V., Nuzhdin, V.I., Valeev, V.F., Osin, Y.N. (2017). Characterization of the Surface of Silver Ion-Implanted Silicon by Optical Reflectance. *Journal of Applied Spectroscopy*, 84(5), 785–789.

[5] Crecelius, G., Radermacher, K., Dieker, Ch. (1993). Reaction of iron and silicon during ion implantation. *Journal of Applied Physics*, 73(10), 4848–4851.

[6] Souza, J.P., Amaral, L. (1992). Recrystallization behavior of silicon implanted with iron. *Journal of Applied Physics*, 71(11), 5423–5426.

[7] Omae, K., Bae, I., Naito, M., Ishimaru, M., Hirotsu, Y., Valdez, J., Sickafus, K. (2006). Structural evolution in Fe ion implanted Si upon thermal annealing. *Nuclear Instruments and Methods in Physics Research B*, 250(1), 300–302.

[8] Markwitz, A., Kant, K., Carder, D., Johnson, P.B. (2009, July). Low-energy Fe+ ion implantation into silicon nanostructures. *AIP Conference Proceedings*, 1151, 149–152.

[9] Yilgin, R., Yurtisigi, M.K., Parabas, A., Turksoy, M., Ozdemir, M., Aktas, B., Kolitsch, A. (2012). Ferromagnetic Behavior of Fe+ Implanted Si (100) Semiconductor. *Journal of superconductivity and novel magnetism*, 25(8), 2731–2735.

[10] Sobolev, N.A., Aleksandrov, O. V., Sakharov, V.I., Serenkov, I.T., Shek, E.I., Kalyadin, A.E., Parshin, O., Melesov, N.S. (2019). Influence of Annealing Temperature on Electrically Active Centers in Silicon Implanted with Germanium Ions. Semiconductors, 53(2), 153–155.

[11] Voelskow, M., Stoimenos, I., Rebohle, L., Skorupa, W. (2011). The formation of near surface SiGe layers with combined high-dose ion implantation and flash-lamp annealing. *Physica Status Solidi C Current Topics*, 8, 960–963.

[12] Gao, K., Prucnal, S., Mücklich, A., Skorupa, W., Zhou, S. (2013). Fabrication of Si 1− x Ge x alloy on silicon by Ge-Ion-implantation and short-time-annealing. *Acta Physica Polonica A*, 123(5), 858–861.

[13] Impellizzeri, G., Mirabella, S., Grimaldi, M. G. (2011). Ion implantation damage and crystalline-amorphous transition in Ge. *Applied Physics A*, 103(2), 323–328.

[14] Dedyulin, S.N., Goncharova, L.V. (2012). Thermal oxidation of Ge-implanted Si: Role of defects. Nuclear Instruments and Methods in Physics Research Section B: *Beam Interactions with Materials and Atoms*, 272, 334–337.

[15] Gauster, W.B., Bushnell, J.C. (1970). Laser-induced infrared absorption in silicon. *Journal of Applied Physics*, 41(9), 3850–3853.

[16] Glunz, S.W., Warta, W. (1995). High-resolution lifetime mapping using modulated free-carrier absorption. *Journal of Applied Physics*, 77(7), 3243–3247.

[17] Glunz, S.W., Sproul, A.B., Warta, W., Wettling, W. (1994). Injection-level-dependent recombination velocities at the Si–SiO2 interface for various dopant concentrations. *Journal of Applied Physics*, 75(3), 1611–1615.

[18] Sanii, F., Giles, F.P., Schwartz, R.J., Gray, J.L. (1992). Contactless nondestructive measurement of bulk and surface recombination using frequency-modulated free carrier absorption. *Solid-State Electronics*, 35(3), 311–317.

[19] Nordal, P.E., Kanstad, S.O. (1979). Photothermal radiometry. *Physica Scripta*, 20(5-6), 659.

[20] Pham Tu Quoc, S., Cheymol, G., Semerok, A. (2014). New contactless method for thermal diffusivity measurements using modulated photothermal radiometry. *Review of Scientific Instruments*, 85(5), 054903.

[21] Kusiak, A., Martan, J., Battaglia, J.L., Daniel, R. (2013). Using pulsed and modulated photothermal radiometry to measure the thermal conductivity of thin films. *Thermochimica Acta*, 556, 1–5.

[22] Pawlak, M., Horny, N., Scholz, S., Ebler, C., Ludwig, A., Wieck, A. D. (2018). Simultaneous measurement of infrared absorption coefficient of carbon doped Al0.33Ga0.67As thin film and thermal boundary resistance between thin film and heavily Zn doped GaAs using spectrally-resolved modulated photothermal infrared radiometry. *Thermochimica Acta*, 667, 73–78.

[23] Pawlak, M., Pal, S., Scholz, S., Ludwig, A., Wieck, A.D. (2018). Simultaneous measurement of thermal conductivity and diffusivity of an undoped Al0. 33Ga0. 67As thin film epitaxially grown on a heavily Zn doped GaAs using spectrally-resolved modulated photothermal infrared radiometry. *Thermochimica Acta*, 662, 69–74.

[24] Chrobak, L., Malinski, M. (2018). Comparison of three nondestructive and contactless techniques for investigations of recombination parameters on an example of silicon samples. *Infrared Physics and Technology*, 91, 1–7.

[25] Malinski, M., Chrobak, L., Madej, W., Kukharchyk, N., Au^{2+}-implanted regions in silicon visualized using a modulated free-carrier absorption method, *International Journal of Thermophysics*, 38(110).

[26] Chrobak, Ł., Malinski, M. (2018). Properties of Silicon Implanted with Fe^{+}, Ge^{+}, Mn^{+} Ions Investigated Using a Frequency Contactless Modulated Free-Carrier Absorption Technique. *Optical Materials*, 86, 484–491.

[27] Malinski, M., Pawlak, M., Pal, S., Ludwig, A. (2015). Monitoring of amorfization of the oxygen implanted layers in silicon wafers using photothermal radiometry and modulated free carrier absorption methods. *Applied Physics A*, 118(3), 1009–1014.

[28] Malinski, M., Pawlak, M. (2014). Measurements of the optical absorption coefficient of Ar8+ ion implanted silicon layers using the photothermal radiometry and the modulated free carrier absorption methods. *Infrared Physics & Technology*, 67, 604–608.

[29] Chrobak, L., Malinski, M. (2019). On Investigations of the Optical Absorption Coefficient of Gold and Germanium Implanted Silicon with the Use of the Non-destructive Contactless Photo Thermal Infrared Radiometry. *Journal of Electronic Materials*, 48(8), 5273–5278.

[30] Fujiwara, H. (2007). *Spectroscopic ellipsometry: principles and applications*. John Wiley & Sons.

[31] Adams, J.R., Bashara, N.M. (1975). Determination of the complex refractive index profiles in $P+_{31}$ ion implanted silicon by ellipsometry. *Surface Science*, 49(2), 441–458.

[32] Lohner, T., Mezey, G., Kotai, E., Paszti, F., Manuaba, A., Gyulai, J. (1983). Characterization of ion implanted silicon by ellipsometry and channeling. *Nuclear Instruments and Methods in Physics Research*, 209, 615–620.

[33] Fried, M., Lohner, T., Aarnink, W.A.M., Hanekamp, L.J., van Silfhout, A. (1992). Determination of complex dielectric functions of ion implanted and implanted-annealed amorphous silicon by spectroscopic ellipsometry. *Journal of Applied Physics*, 71(10), 5260–5262.

[34] Giri, P. K., Tripurasundari, S., Raghavan, G., Panigrahi, B.K., Magudapathy, P., Nair, K.G.M., Tyagi, A.K. (2001). Crystalline to amorphous transition and band structure evolution in ion-damaged silicon studied by spectroscopic ellipsometry. Journal of Applied Physics, 90(2), 659–669.

[35] Kurihara, K., Hikino, S.I., Adachi, S. (2004). Optical properties of N+ ion-implanted and rapid thermally annealed Si (100) wafers studied by spectroscopic ellipsometry. *Journal of Applied Physics*, 96(6), 3247–3254.

[36] Petrik, P., Polgár, O., Fried, M., Lohner, T., Khánh, N.Q., Gyulai, J. (2003). Ellipsometric characterization of damage profiles using an advanced optical model. *Journal of Applied Physics*, 93(4), 1987–1990.

[37] Petrik, P. (2008). Ellipsometric models for vertically inhomogeneous composite structures. *Physica Status Solidi (A) Applications and Materials Science*, 205(4), 732–738.

[38] Dorywalski, K., Andriyevsky, B., Piasecki, M., Kityk, I. (2017). Parametrized optical functions of strontium barium niobate crystals in the vacuum ultraviolet spectral range. *Journal of Applied Physics*, 122(11).

Metrol. Meas. Syst., Vol. 27 (2020), No. 2, pp. 323–337
DOI: 10.24425/mms.2020.132778

[39] Dorywalski, K., Lemée, N., Andriyevsky, B., Schmidt-Grund, R., Grundmann, M., Piasecki, M., Bousquet, M., Krzyzynski, T. (2017). Optical properties of epitaxial $Na_{0.5}Bi_{0.5}TiO_3$ lead-free piezoelectric thin films: ellipsometric and theoretical studies. *Applied Surface Science*, 421, 367–372.

[40] Dorywalski, K., Andriyevsky, B., Piasecki, M., Lemee, N., Patryn, A., Cobet, C., Esser, N. (2013). Ultraviolet vacuum ultraviolet optical functions for $SrTiO_3$ and $NdGaO_3$ crystals determined by spectroscopic ellipsometry. *Journal of Applied Physics*, 114 (4), 043513.

[41] Andriyevsky, B., Piasecki, M., Dorywalski, K., Cobet, C., Esser, N., Świrkowicz, M., Majchrowski, A., Jaroszewicz, L.R., Kityk, I.V. (2013). Specific features of Yb^{3+} ions in electronic band structure and optical functions of $RbNd(WO_4)_2$ crystals: synchrotron ellipsometry measurement and DFT simulations, *Journal of Alloys and Compounds*, 577, 237–246.

[42] Dorywalski, K., Andriyevsky, B., Cobet, C., Piasecki, M., Kityk, I.V., Esser, N., Łukasiewicz, T., Patryn, A. (2013). Ellispometric study of near band gap optical properties of $Sr_xBa_{1-x}Nb_2O_6$ crystals. *Optical Materials*. 35(5), 887–892

[43] Azzam R.M.A., Bashara N.B. (1987). *Ellipsometry and polarized light*, Amsterdam: North-Holland Pub. Co.

[44] Shamiryan, D., Likhachev, D.V. (2012). Ion Implantation. Goorsky, M. (eds.). *Spectroscopic ellipsometry of ion-implantation-induced damage*. Rijeka: InTech, 89-104.

[45] Radisic, D., Shamiryan, D., Mannaert, G., Boullart, W., Rosseel, E., Bogdanowicz, J., Goossens, J., Marrant, K., Bender, H., Sonnemans, R., Berry, I. (2009). Metrology for implanted Si substrate and dopant loss studies. *ECS Transactions*, 25(5), 367–374.

[46] Radisic, D., Shamiryan, D., Mannaert, G., Boullart, W., Rosseel, E., Bogdanowicz, J., Goossens, J., Marrant, K., Bender, H., Sonnemans, R., Berry, I. (2010). Metrology for implanted Si substrate loss studies, *Journal of Electrochemical Society*, 157 (5), H580–H584.

[47] Shamiryan, D., Radisic, D., Boullart, W. (2010). In-line control of Si loss after post ion implantation strip. *Microelectronic engineering*, 87(9), 1669–1673.

[48] Webb, A.P., Townsend, P.D. (1976). Refractive index profiles induced by ion implantation into silica. *Journal of Physics D: Applied Physics*, 9(9), 1343–1354.

[49] Jellison Jr, G.E., Modine, F.A. (1996). Parameterization of the optical functions of amorphous materials in the interband region. *Applied Physics Letters*, 69(3), 371–373.

[50] Ferlauto, A.S., Ferreira, G.M., Pearce, J.M., Wronski, C. R., Collins, R.W., Deng, X., Ganguly, G. (2002). Analytical model for the optical functions of amorphous semiconductors from the near-infrared to ultraviolet: Applications in thin film photovoltaics. *Journal of Applied Physics*, 92(5), 2424–2436.

[51] Herzinger, C.M., Johs, B., McGahan, W.A., Woollam, J.A., Paulson, W. (1998). Ellipsometric determination of optical constants for silicon and thermally grown silicon dioxide via a multi-sample, multi-wavelength, multi-angle investigation. *Journal of Applied Physics*, 83(6), 3323–3336.

[52] Hale, J., Johs, B. (2011). *CompleteEASE™ Data Analysis Manual*. Lincoln: J.A. Woollam Co.